A Novel INS/GPS Fusion Architecture for Aircraft Navigation

Venkatesh K. Madyastha, Vishal Cholapadi Ravindra, S.M. Vaitheeswaran
National Aerospace Laboratories
Bangalore 560017, Karnataka, India
Email: venky107@gmail.com, vishalcr, smvaithu@nal.res.in

Srinath Mallikarjunan
Unmanned Dynamics
Chennai 600006, Tamil Nadu, India
Email: srinath@unmanned-dynamics.com

***Abstract*—In this paper, we address the issue of aircraft navigational state estimation from the perspective of (i) aircraft attitude estimation, also called as the attitude heading reference system (AHRS), and (ii) estimating the full inertial solution of the aircraft (position, velocity & attitude), also known as inertial navigation system-global positioning system (INS/GPS) fusion, in the presence of accelerometer and gyroscopic bias. A suite of nonlinear filters; two Kalman filter (KF) based — extended and unscented Kalman filter (EKF, UKF) and a non-KF based filter that is the nonlinear complementary filter (NCF) on the $SO(3)$ group, are studied and evaluated for the AHRS. In this paper we propose a novel INS/GPS fusion architecture that demonstrated a significant improvement in performance over the conventional KF based schemes, in tests done on realistic simulated aircraft data. In the proposed architecture, the attitude estimation is decoupled from the position and velocity estimation, by exploiting the NCF as it is known for its superior attitude and gyroscopic bias estimation performance. The position and velocity estimation is carried out by a conventional EKF. The crucial difference between KF based schemes and the NCF for attitude estimation is in the generation of the measurement set, which involves trigonometric inverses and are susceptible to singularities for KF based schemes, which the NCF avoids. Furthermore, the NCF algorithm is faster and computationally more efficient than a KF algorithm scheme since the NCF *does not* involve the computation of matrix inverses like KF based schemes.**

I. Introduction

The problem of real-time attitude and heading estimation of unmanned aerial vehicles (UAVs) is one that has been widely studied as an attitude heading reference system (AHRS). Inertial sensors of the microelectromechanical systems (MEMS) type such as rate gyroscopes, accelerometers, and heading sensors such as magnetometers are used to respectively measure instantaneous angular velocities, specific forces and heading of UAVs [31]. The suite of inertial sensors constitute an inertial measurement unit (IMU), which is widely used in an inertial navigation system (INS) for applications such as air vehicle navigation and outdoor robotics [14], [25]. The INS calculates, via dead reckoning, the estimates of the vehicle orientation, position and velocity without the need for an external reference [31]. The drawback of the INS is that it suffers from *drift* since this form of navigation integrates the inertial sensor outputs to get the orientation and position of the vehicle, given a known initial condition. These drifts are significant in the case of small UAVs, as MEMS based inertial sensors are used due to them being low-cost and low-weight. However, these MEMS based sensors are known to suffer biases and high noise levels [32], and hence need to be corrected via an external reference system. Typically, INS outputs are corrected via the global positioning system (GPS), as it provides reliable location and velocity components at all times and anywhere on or near the Earth, when and where there is an unobstructed line of sight to four or more GPS satellites [27], [28]. This fusion is typically performed through nonlinear filtering; a detailed literature survey of the various schemes for aircraft attitude estimation can be found in [2].

The design of nonlinear filters is a very challenging problem that has received a considerable amount of attention in the literature over the past few decades [3], [8]. Of the numerous attempts being made for the development of nonlinear filters, the extended Kalman filter (EKF) is the earliest and the most prevalent approach. The design of the EKF is based on a first order local linearization of the system around the current state estimate at each time step [4], [5], [13]. The first ever implementation of an EKF is credited to Peter Swerling [16], [29]. The well known KF [23] equations can then be applied to the linearized system to compute the Kalman gain and the covariance matrices. Although easy to implement, a major limitation of the standard EKF is that it approximates the expected value of a nonlinear function $f(x)$ as a function of the expected value. To address the limitations inherent in an EKF, the unscented Kalman filter (UKF) [21] was developed, which neither relies on the linearization steps required by the EKF nor the computation of Jacobian matrices. Instead, the UKF utilizes the fact that it is easier to approximate a Gaussian distribution than it is to approximate an arbitrary nonlinear function or transformation [22].

Quaternion representations of the attitude kinematics, particularly in the estimation and control of satellite systems, was a key step addressed for the development of robust filters that addressed the issue of gyroscopic bias [18], [26], [30]. In [15], a nonlinear invariant attitude observer is proposed directly on the special orthogonal group,[1] denoted as $SO(3)$. Recently, a nonlinear complementary filter (NCF) that formulates the

[1]The special orthogonal group, also called proper orthogonal group, is the transformation matrix whose determinant is unity.

filtering problem as a deterministic observer, with kinematics posed directly on the $SO(3)$ group driven by reconstructed attitude and angular velocity measurements was proposed in [7]. This estimation scheme estimates the body-to-inertial frame rotation matrix from which the aircraft attitude estimates are derived. Unlike the EKF or the UKF, the NCF does not require all sources of gyroscopic bias to be modeled in the filter state vector, rather it lumps all sources of bias together and estimates this consolidated bias. For example, in aircraft attitude estimation from noisy and biased sensors such as rate gyroscopes, all sources of bias need to be modeled in the state vector for the EKF or the UKF to perform reasonably well. Thus, as the number of sources of bias increases, so does the dimension of the filter state vector. The NCF relies on the fact that the accelerometer provides a reasonable approximation of the gravitational force, thereby performing the job of a gravity sensor. Thus, the accelerometer along with a magnetometer, that measures the inertial magnetic field, is used to form a set of orthogonal measurements for the NCF implementation.

This paper studies two problems which are (i) Aircraft attitude estimation, and (ii) Aircraft inertial navigation. The **aircraft attitude estimation** problem involves estimating the attitude and heading via accelerometers, rate gyroscopes, magnetometers and GPS. *The key issue addressed here is the online estimation of rate gyroscopic bias*. Several known sources of bias such as angle random walk, rate random walk and colored noise [32] are considered in the simulated gyroscope model. However, in the real world, it is unreasonable to assume that all bias sources are known, and hence, modeled. Furthermore, since for small UAVs, computational simplicity is paramount, there is a need to reduce the dimensionality of the filter without compromising on the performance. This paper, to the best of our knowledge, is the first to compare the performance of two KF based estimators and a nonlinear complementary filtering scheme for UAV attitude estimation. Furthermore, this paper is the first to analyze the performance of the aforementioned filters under the condition of unmodeled bias.[2] Thus, the objective of this paper is to identify the nonlinear filtering scheme on which a real world AHRS should be based that accounts for the various unmodeled sources of *gyroscopic bias* while not increasing the dimensionality of the filter model. Furthermore, we give a detailed explanation for excluding accelerometer bias from the framework of attitude estimation *only*. The **aircraft inertial navigation** problem is considered in this paper from the perspective of splitting the inertial states of the problem into two sets: (i) attitude and rate gyroscopic bias states, and (ii) position, velocity and accelerometer bias states. The attitude and rate gyroscopic bias states are estimated via an NCF while the position, velocity and accelerometer bias states are estimated via an EKF[3]. ***To the best of our knowledge, this is the first paper to propose a novel INS/GPS fusion architecture by exploiting the robustness characteristics of the NCF scheme.***

[2]Unmodeled bias $\Rightarrow$ those bias sources **present** in the gyro model but *deliberately* excluded from the filter model, hence not specifically estimated.

[3]Instead of an EKF, a UKF could be designed to estimate the position, velocity and accelerometer states.

The rest of the paper is structured as follows: Section II presents the AHRS and the INS/GPS process and measurement models. Section III presents the filtering methodologies while Section IV presents some simulations and results for the models developed in Section II. Finally, Section V contains some concluding remarks. Appendix A addresses the issue of nonlinear observability in an AHRS formulation from the perspective of ignoring accelerometer bias. Throughout the paper, small letters are used for scalars, bold symbols for vectors, capital letters for matrices, $(\mathbf{a})_\times$ denotes the skew symmetric matrix representation of the vector $\mathbf{a}$ and $(M)^T$ denotes the transpose of the matrix M.

II. Aircraft Models for Estimation

We describe the AHRS and the INS/GPS models.

A. Attitude Heading Reference System (AHRS)

A typical AHRS for a small UAV consists of triaxial MEMS gyroscopes, accelerometers and magnetometers [24] and typically augmented by a GPS receiver.

1) Rate Gyroscope Model: The rate gyroscope measurements $p_m,\ q_m,\ r_m$ are assumed to be modeled as [32]:

$$\begin{aligned} p_m &= p + b_{0_p} + b_{1_p} + b_{2_p} + w_p \\ q_m &= q + b_{0_q} + b_{1_q} + b_{2_q} + w_q \\ r_m &= r + b_{0_r} + b_{1_r} + b_{2_r} + w_r \end{aligned} \tag{1}$$

where, $p,\ q,\ r$ are the **true** values of the angular velocity; $b_{0_p},\ b_{0_q},\ b_{0_r}$ are the *constant* bias terms, $b_{1_p},\ b_{1_q},\ b_{1_r}$ are the *rate random walk* bias components, $b_{2_p},\ b_{2_q},\ b_{2_r}$ are the *colored noise* bias components and $w_p,\ w_q,\ w_r$ denote the error due to *sampling noise* and are typically modeled as zero mean, band-limited, additive white Gaussian noise (AWGN) processes of covariances denoted by $\sigma_p^2, \sigma_q^2, \sigma_r^2$, respectively.

Remark 2.1: The effects due to $b_{0_p},\ b_{0_q},\ b_{0_r}$ can be estimated off-line and removed from the rate gyroscope output.

Remark 2.2: The time varying rate random walk bias components can be modeled as Weiner processes given by $\dot{b}_{1_p} = w_{1_p},\ \dot{b}_{1_q} = w_{1_q},\ \dot{b}_{1_r} = w_{1_r}$, where $w_{1_p}, w_{1_q}, w_{1_r}$ are zero mean, band-limited AWGN processes with covariances denoted by $\sigma_{1_p}^2, \sigma_{1_q}^2, \sigma_{1_r}^2$, respectively.

Remark 2.3: The effects due to correlated noise can be modeled as first order Gauss-Markov processes [1]; $\dot{b}_{2_p} = -\frac{b_{2_p}}{\tau} + \frac{w_{2_p}}{\tau},\ \dot{b}_{2_q} = -\frac{b_{2_q}}{\tau} + \frac{w_{2_q}}{\tau},\ \dot{b}_{2_r} = -\frac{b_{2_r}}{\tau} + \frac{w_{2_r}}{\tau}$, where $w_{2_p},\ w_{2_q},\ w_{2_r}$ represent the driving process noise components which are assumed to be zero mean, band-limited AWGN processes with covariances denoted by $\sigma_{2_p}^2, \sigma_{2_q}^2, \sigma_{2_r}^2$, respectively, with τ denoting the time constant of the process.

Remark 2.4: We model only constant bias in the filter while treating the other sources of bias as *unmodeled* since augmenting all bias sources as states in the filter model without additional measurements can lead to loss of observability and adversely affect the filter stability. Thus $b_{1_p}, b_{1_q}, b_{1_r}$ are included as states in the filter model while $b_{2_p}, b_{2_q}, b_{2_r}$ are treated as *unmodeled* states.

2) Accelerometer Model: A triaxial accelerometer measures the proper acceleration (acceleration relative to free-fall), in terms of g-force. These accelerometer readings are denoted as $a_{x_m},\ a_{y_m},\ a_{z_m}$ and are given by

$$a_{x_m} = a_x + w_{a_x}, \quad a_{y_m} = a_y + w_{a_y}, \quad a_{z_m} = a_z + w_{a_z} \quad (2)$$

where, $a_x,\ a_y,\ a_z$ are the **true** forces and $w_{a_x},\ w_{a_y},\ w_{a_z}$ denote the additive sensor noise processes, respectively, for the $x,\ y,\ z$ axes and are modeled as zero mean, band-limited AWGN processes with covariances denoted by $\sigma^2_{a_x},\ \sigma^2_{a_y},\ \sigma^2_{a_z}$, respectively.

Remark 2.5: Accelerometer bias is not considered since it is not observable in an AHRS formulation. For a detailed explanation refer to Appendix A. In case accelerometer biases are significant, an INS-GPS filter must be designed [31].

3) AHRS Process Model: Denote $s_* \equiv \sin(*),\ c_* \equiv \cos(*),\ t_* \equiv \tan(*)$. Consider the system of differential equations which describe the aircraft attitude[4] parameterized via Euler angles as [19]:

$$\underbrace{\frac{d}{dt}\begin{bmatrix}\psi\\ \theta\\ \phi\end{bmatrix}}_{\dot{\boldsymbol{\xi}}} = \underbrace{\begin{bmatrix}0 & \frac{s_\phi}{c_\theta} & \frac{c_\phi}{c_\theta}\\ 0 & c_\phi & -s_\phi\\ 1 & s_\phi t_\theta & c_\phi t_\theta\end{bmatrix}}_{\Lambda}\underbrace{\begin{bmatrix}p_m\\ q_m\\ r_m\end{bmatrix}}_{\boldsymbol{\omega}_m}, \Rightarrow \dot{\boldsymbol{\xi}} = \Lambda\boldsymbol{\omega}_m \quad (3)$$

where, $\psi,\ \theta,\ \phi$ are the Euler angles (yaw, pitch and roll) that describe the aircraft attitude and $\boldsymbol{\omega}_m$ denotes the vector of the *measured* aircraft body angular rates. Denote $\mathbf{b}_1 = \begin{bmatrix} b_{1_p} & b_{1_q} & b_{1_r}\end{bmatrix}^T$, $\mathbf{b}_2 = \begin{bmatrix} b_{2_p} & b_{2_q} & b_{2_r}\end{bmatrix}^T$, $\mathbf{w} = \begin{bmatrix} w_p & w_q & w_r\end{bmatrix}^T$, $\mathbf{w}_1 = \begin{bmatrix} w_{1_p} & w_{1_q} & w_{1_r}\end{bmatrix}^T$ and $\mathbf{w}_2 = \begin{bmatrix} w_{2_p} & w_{2_q} & w_{2_r}\end{bmatrix}^T$. Substituting Eq. (1) into Eq. (3) and using Remark 2.4, the AHRS process equations are:

$$\underbrace{\begin{bmatrix}\dot{\boldsymbol{\xi}}\\ \dot{\mathbf{b}}_1\end{bmatrix}}_{\dot{\mathbf{x}}} = \underbrace{\begin{bmatrix}0_3 & \Lambda\\ 0_3 & 0_3\end{bmatrix}\begin{bmatrix}\boldsymbol{\xi}\\ \mathbf{b}_1\end{bmatrix} + \Gamma_B\boldsymbol{\omega} + \Gamma\bar{\mathbf{w}} + \Gamma_B\mathbf{b}_2}_{\mathbf{f}} \quad (4)$$

where, $\Gamma = \begin{bmatrix}\Lambda & 0_3\\ 0_3 & I_3\end{bmatrix}$, 0_3 denotes a 3×3 zero matrix, I_3 denotes a 3×3 identity matrix, $\Gamma_B = \begin{bmatrix}\Lambda\\ 0_3\end{bmatrix}$ and $\bar{\mathbf{w}} = \begin{bmatrix}\mathbf{w}^T & \mathbf{w}_1^T\end{bmatrix}^T$ and the term $\Gamma_B\mathbf{b}_2$ represents the unmodeled dynamics vector (**neglected in the filter process model**).

4) AHRS Measurement Model: Consider the **force equations** for a 6 DOF aircraft as [19]:

$$\begin{bmatrix}a_{x_m}\\ a_{y_m}\\ a_{z_m}\end{bmatrix} = \begin{bmatrix}\dot{u}^E\\ \dot{v}^E\\ \dot{w}^E\end{bmatrix} + \begin{bmatrix}q_m w^E - r_m v^E\\ r_m u^E - p_m w^E\\ p_m v^E - q_m u^E\end{bmatrix} + g\begin{bmatrix}s_\theta\\ -c_\theta s_\phi\\ -c_\theta c_\phi\end{bmatrix} \quad (5)$$

where $a_{x_m} = \frac{X}{m}, a_{y_m} = \frac{Y}{m}, a_{z_m} = \frac{Z}{m}$, and $X,\ Y,\ Z$ are the components of the resultant aerodynamic force acting on the aircraft in body axis frame; $\left(u^E,\ v^E,\ w^E\right)$ are the components of the GPS obtained aircraft ground speed expressed in the body frame; $\left(\dot{u}^E,\ \dot{v}^E,\ \dot{w}^E\right)$ are the aircraft linear accelerations expressed in the body frame; m is the mass of the aircraft, and g is the acceleration due to gravity. The terms $a_{x_m}, a_{y_m}, a_{z_m}$ are the accelerometer readings in the body frame and are given by Eq. (2). The pitch and roll measurements are obtained as:

$$\theta_m = \sin^{-1}\left(\frac{a_{x_m} - \dot{u}^E + r_m v^E - q_m w^E}{g}\right) \quad (6)$$

$$\phi_m = \tan^{-1}\left(\frac{a_{y_m} - \dot{v}^E + p_m w^E - r_m u^E}{a_{z_m} - \dot{w}^E + q_m u^E - p_m v^E}\right) \quad (7)$$

Furthermore, a magnetometer[5] is used to generate the aircraft heading measurement.

Remark 2.6: The quantities u^E, v^E, w^E in Eqs. (6) and (7) are obtained as $\begin{bmatrix}u^E & v^E & w^E\end{bmatrix}^T = \mathcal{R}_I^B\begin{bmatrix}\dot{x}_{gps} + w_{x_{gps}} & \dot{y}_{gps} + w_{y_{gps}} & \dot{z}_{gps} + w_{z_{gps}}\end{bmatrix}^T$, where, $\mathcal{R}_I^B$ denotes the direction cosine matrix[6] that takes a vector from the inertial to the body frame, $\dot{x}_{gps},\ \dot{y}_{gps},\ \dot{z}_{gps}$ denote the aircraft velocity components in the inertial frame provided by an on-board GPS [11] receiver at an update rate of f_u Hz and $w_{x_{gps}}, w_{y_{gps}}, w_{z_{gps}}$ denote zero mean, band-limited AWGN processes of covariances denoted by $\sigma^2_{x_{gps}}, \sigma^2_{y_{gps}}, \sigma^2_{z_{gps}}$, respectively. Furthermore, $\dot{u}^E, \dot{v}^E, \dot{w}^E$ can be obtained by finite differencing[7] u^E, v^E, w^E, given f_u.

B. Inertial Navigation/Global Positioning System (INS/GPS)

We recall the rate gyro and accelerometer models used.

Remark 2.7: The rate gyroscope model used is similar to the model used in Eq. (1), with the bias terms modeled as shown in Remarks 2.2 and 2.3. The accelerometer model for the INS/GPS problem is given as $a_{x_m} = a_x + b_{a_x} + w_{a_x}, a_{y_m} = a_y + b_{a_y} + w_{a_y}, a_{z_m} = a_z + b_{a_z} + w_{a_z}$, where, $b_{a_x}, b_{a_y}, b_{a_z}$, are constant bias offsets, $a_x,\ a_y,\ a_z$ are the **true** forces and $w_{a_x},\ w_{a_y},\ w_{a_z}$ denote the additive sensor noise processes, respectively, for the $x,\ y,\ z$ axes and are modeled as zero mean, band-limited AWGN processes with covariances denoted by $\sigma^2_{a_x},\ \sigma^2_{a_y},\ \sigma^2_{a_z}$, respectively. *The constant bias offsets are modeled as Weiner processes similar to Remark 2.2.* Thus the final state vector includes (λ, μ, h), (v_n, v_e, v_d), (ψ, θ, ϕ), $\left(b_{1_p}, b_{1_q}, b_{1_r}\right)$ and $\left(b_{a_x}, b_{a_y}, b_{a_z}\right)$. Denote $\mathbf{w}_a = \begin{bmatrix} w_{a_x} & w_{a_y} & w_{a_z}\end{bmatrix}^T$.

Neglecting the effect of Earth's rotation rate, the INS/GPS model in the local North-East-Down (NED) frame[8] is [31]:

$$\underbrace{\begin{bmatrix}\dot{\lambda}\\ \dot{\mu}\\ \dot{h}\end{bmatrix}}_{\dot{\mathbf{p}}_I} = \underbrace{\begin{bmatrix}\frac{v_n}{R_M + h}\\ \frac{v_e}{(R_N + h)c_\lambda}\\ -v_d\end{bmatrix}}_{\mathbf{f}_1}, \quad \begin{array}{c} R_M = R_0\left(1 - e^2\right)/\gamma^3\\ R_N = R_0/\gamma\\ \gamma = \sqrt{1 - e^2 s_\lambda^2}\end{array}$$

[4] For the full set of aircraft equations in the body frame, refer [19].

[5] A magnetometer measures the strength and direction of the magnetic field in its vicinity.

[6] $\mathcal{R}_I^B$ is obtained using the current online attitude estimates.

[7] If the GPS obtained velocity is prohibitively noisy, then their low pass filtered (or smoothed) outputs can be used for the finite differencing instead.

[8] Locally, the North East Down (NED) frame is assumed to be inertial.

$$\underbrace{\begin{bmatrix}\dot{v}_n\\ \dot{v}_e\\ \dot{v}_d\end{bmatrix}}_{\dot{\mathbf{v}}_I} = \underbrace{\mathcal{R}_B^I\begin{bmatrix}a_x+b_{a_x}\\ a_y+b_{a_y}\\ a_z+b_{a_z}\end{bmatrix}+\begin{bmatrix}\frac{v_nv_d}{R_M+h}-\frac{v_e^2t_\lambda}{R_N+h}\\ \frac{v_e(v_d+v_nt_\lambda)}{R_N+h}\\ \frac{-v_d^2}{R_M+h}-\frac{v_e^2}{R_N+h}+g\end{bmatrix}}_{\mathbf{f}_2}+\mathcal{R}_B^I\mathbf{w}_a$$

$$\dot{\boldsymbol{\xi}} = \Lambda\boldsymbol{\omega}_m \tag{8}$$

where, $\lambda,\ \mu,\ h$ denote position (latitude, longitude and altitude), $v_n,\ v_e,\ v_d$ denote velocity, $\psi,\ \theta,\ \phi$ denote heading, pitch & roll, R_M, R_N respectively denote the Earth's meridional and normal radius of curvature, $R_0 \approx 6378137m, e = 0.01671123$ denote the Earth's radius and eccentricity respectively, g denotes the acceleration due to gravity and $\mathcal{R}_B^I = \left(\mathcal{R}_I^B\right)^T = \begin{bmatrix} c_\theta c_\psi & s_\phi s_\theta c_\psi - c_\phi s_\psi & c_\phi s_\theta c_\psi + s_\phi s_\psi \\ c_\theta s_\psi & s_\phi s_\theta s_\psi + c_\phi c_\psi & c_\phi s_\theta s_\psi - s_\phi c_\psi \\ -s_\theta & s_\phi c_\theta & c_\phi c_\theta \end{bmatrix}$.

Remark 2.8: The measurement model consists of GPS position, velocity and heading derived from a magnetometer.

III. Filter Methodologies

We present the outlines of two KF based estimation methodologies and one non-KF based filtering methodology.

1) Extended Kalman Filter (EKF): The design of the EKF is accomplished in two stages, which are (i) Prediction and (ii) Update. Denoting $\hat{\mathbf{x}}_k^-$ and $\hat{\mathbf{x}}_k$ as, respectively, the predicted and corrected state estimates at k, the prediction ($9 \sim 10$) and update ($11 \sim 13$) steps are [17]:

$$\dot{\hat{\mathbf{x}}} = \hat{\mathbf{f}}, \quad \dot{P} = FP + PF^T + \Gamma Q \Gamma^T \tag{9}$$

$$\hat{\mathbf{x}}_k^- = \hat{\mathbf{x}}_{k-1} + \dot{\hat{\mathbf{x}}}\Delta t, \quad P_k^- = P_{k-1} + \dot{P}\Delta t \tag{10}$$

$$K_k = P_k^- H_k^T \left(H_k P_k^- H_k^T + R_k\right)^{-1} \tag{11}$$

$$\hat{\mathbf{x}}_k = \hat{\mathbf{x}}_k^- + K_k\left(\mathbf{z}_k - \mathbf{h}\left(\hat{\mathbf{x}}_k^-\right)\right) \tag{12}$$

$$P_k = \left(I - K_k H_k\right) P_k^- \tag{13}$$

where, $\hat{\mathbf{f}}, \Gamma$ are evaluated at $\hat{\mathbf{x}}_{k-1}$; $F = \left.\frac{\partial \mathbf{f}}{\partial \mathbf{x}}\right|_{\mathbf{x}=\hat{\mathbf{x}},\boldsymbol{\omega}_m}$, $H_k = \left.\frac{\partial \mathbf{h}(\mathbf{x}_k)}{\partial \mathbf{x}_k}\right|_{\mathbf{x}_k=\hat{\mathbf{x}}_k^-}$ denote the Jacobians; $\mathbf{h}\left(\hat{\mathbf{x}}_k^-\right)$ denotes the measurement evaluated at $\hat{\mathbf{x}}_k^-$; K_k denotes the Kalman gain; P_k^-, P_k denote the predicted and corrected state error covariance matrices; Q, R_k denote the process and measurement noise intensity matrices and Δt denotes the simulation time step. The vectors $\mathbf{x}, \mathbf{f}$ and the matrices F and Γ for the AHRS and INS/GPS formulations are shown in Appendix B.

2) Unscented Kalman Filter (UKF): The UKF is based on propagating the mean and covariance through a nonlinear transformation called the *unscented transform* [21], which is a novel method for calculating the statistics of a random variable that undergoes a nonlinear transformation. The typical additive UKF steps are [10]:

1) Initialize the state estimate as $\hat{\mathbf{x}}_0 = \hat{\mathbf{x}}(0) = E[\mathbf{x}_0]$ and the state error covariance matrix as $P_0 = P(0) = E\left[(\mathbf{x}_0 - \hat{\mathbf{x}}_0)(\mathbf{x}_0 - \hat{\mathbf{x}}_0)^T\right]$.
2) For $k = \{1, 2, \ldots, \infty\}$
   i. **Sigma Points**: Calculate the sigma points $\boldsymbol{\chi}_{k-1}$, based on $\hat{\mathbf{x}}_{k-1}$ and P_{k-1}, as $(\boldsymbol{\chi}_{k-1})_0 = \hat{\mathbf{x}}_{k-1}$ and $\boldsymbol{\chi}_{k-1} = \left\{\hat{\mathbf{x}}_{k-1} + \gamma\left(\sqrt{P_{k-1}}\right)_j,\ \hat{\mathbf{x}}_{k-1} - \gamma\left(\sqrt{P_{k-1}}\right)_j\right\}$ where, $j = 1, \ldots, n$, $\gamma = \sqrt{n+\lambda}$ and $\lambda = \alpha^2(n+\kappa) - n$ such that $10^{-4} \leq \alpha \leq 1$, where α determines the spread of the sigma points around the mean, κ is a secondary scaling parameter and n denotes the number of states.
   ii. **Prediction**:
      a. Propagate $\boldsymbol{\chi}_{k-1}$ to obtain the predicted sigma points as $\left(\boldsymbol{\chi}_k^-\right)_i = \mathbf{f}(\boldsymbol{\chi}_{k-1})_i$, $i = 0, \ldots, 2n$.
      b. Obtain the predicted state estimate $\hat{\mathbf{x}}_k^-$ as $\hat{\mathbf{x}}_k^- = \sum_{i=0}^{2n} W_i^{(m)}\left(\boldsymbol{\chi}_k^-\right)_i$, where, $W_0^{(m)} = \frac{\lambda}{n+\lambda}$ and $W_i^{(m)} = \frac{0.5}{n+\lambda}$.
      c. Obtain the predicted state error covariance matrix $P_k^- = \sum_{i=0}^{2n} W_i^{(c)}\left(\boldsymbol{\chi}_k^- - \hat{\mathbf{x}}_k^-\right)_i\left(\boldsymbol{\chi}_k^- - \hat{\mathbf{x}}_k^-\right)_i^T + \Gamma Q \Gamma^T$, where, $W_0^{(c)} = \frac{\lambda}{n+\lambda} + \left(1 - \alpha^2 + \beta\right)$ and $W_i^{(c)} = \frac{0.5}{n+\lambda}$, where β is used to incorporate prior knowledge of the distribution of $\mathbf{x}$ ($\beta = 2$ for Gaussian is optimal).
      d. Re-calculate the sigma points based on $\hat{\mathbf{x}}_k^-$ and P_k^- to incorporate the effect of process noise as $(\boldsymbol{\chi}_k)_0 = \hat{\mathbf{x}}_k^-$ and $\boldsymbol{\chi}_k = \left\{\hat{\mathbf{x}}_k^- + \gamma\left(\sqrt{P_k^-}\right)_j,\ \hat{\mathbf{x}}_k^- - \gamma\left(\sqrt{P_k^-}\right)_j\right\}$.
      e. Propagate $\boldsymbol{\chi}_k$ through $\mathbf{h}(\cdot)$ to obtain the predicted measurement sigma points, $\left(\boldsymbol{\mathcal{Y}}_k^-\right)_j = \mathbf{h}(\boldsymbol{\chi}_k)_j$.
      f. Compute the predicted measurement as $\hat{\mathbf{y}}_k^- = \sum_{i=0}^{2n} W_i^{(m)}\left(\boldsymbol{\mathcal{Y}}_k^-\right)_i$.
   iii. **Correction**: Compute the following:
      a. Covariance of the innovations, $P_{\hat{\mathbf{y}}_k\hat{\mathbf{y}}_k} = \sum_{i=0}^{2n} W_i^{(c)}\left(\boldsymbol{\mathcal{Y}}_k^- - \hat{\mathbf{y}}_k^-\right)_i\left(\boldsymbol{\mathcal{Y}}_k^- - \hat{\mathbf{y}}_k^-\right)_i^T + R_k$.
      b. Cross covariance between $\hat{\mathbf{x}}_k^-$ and $\hat{\mathbf{y}}_k^-$ as $P_{\hat{\mathbf{x}}_k^-\hat{\mathbf{y}}_k} = \sum_{i=0}^{2n} W_i^{(c)}\left(\boldsymbol{\chi}_k - \hat{\mathbf{x}}_k^-\right)_i\left(\boldsymbol{\mathcal{Y}}_k^- - \hat{\mathbf{y}}_k^-\right)_i^T$.
      c. Kalman gain, $K_k = P_{\hat{\mathbf{x}}_k^-\hat{\mathbf{y}}_k} P_{\hat{\mathbf{y}}_k\hat{\mathbf{y}}_k}^{-1}$.
      d. Corrected state estimate at k as $\hat{\mathbf{x}}_k = \hat{\mathbf{x}}_k^- + K_k\left(\mathbf{z}_k - \hat{\mathbf{y}}_k^-\right)$, where, $\mathbf{z}_k$ denotes the actual measurement.
      e. Corrected state error covariance matrix, $P_k = P_k^- - K_k P_{\hat{\mathbf{y}}_k\hat{\mathbf{y}}_k} K_k^T$.
3) Repeat Step 2 till the end of the simulation.

3) Nonlinear Complementary Filter (NCF): The NCF estimates the inertial to body frame rotation matrix from which the aircraft attitude estimates are calculated. Denoting the rotation matrix from inertial to body frame as $\mathcal{R}_I^B$, the following rotation kinematics can be written [7]:

$$\dot{\mathcal{R}}_I^B = \mathcal{R}_I^B(\boldsymbol{\omega}_m)_\times, \quad (\boldsymbol{\omega}_m)_\times = \begin{bmatrix} 0 & -r_m & q_m \\ r_m & 0 & -p_m \\ -q_m & p_m & 0 \end{bmatrix} \tag{14}$$

where, $\mathcal{R}_I^B \in SO(3)$ and $\boldsymbol{\omega}_m$ is given in Eq. (1). Denote $\mathbf{a}_m^B$ and $\boldsymbol{\psi}_m^B$ as the body accelerometer and magnetometer measurements that are related to the inertial measurements as $\mathbf{a}_m^B = \mathcal{R}_I^B\mathbf{a}_m^I + \mathbf{w}_a$, $\boldsymbol{\psi}_m^B = \mathcal{R}_I^B\boldsymbol{\psi}_m^I + \mathbf{w}_\psi$, where, $\mathbf{w}_\psi = \begin{bmatrix} w_{\psi_x} & w_{\psi_y} & w_{\psi_z} \end{bmatrix}^T$ such that $w_{\psi_x}, w_{\psi_y}, w_{\psi_z}$ are zero mean, band-limited AWGN processes of covariances denoted by $\sigma_{\psi_x}^2, \sigma_{\psi_y}^2, \sigma_{\psi_z}^2$. Let the NCF dynamics be

$$\dot{\hat{\mathcal{R}}}_I^B = \hat{\mathcal{R}}_I^B\left(\left(\boldsymbol{\omega}_m - \hat{\mathbf{b}}\right)_\times + k_P(\mathbf{y}_m)_\times\right), \quad \hat{\mathcal{R}}_I^B(0) = \hat{\mathcal{R}}_{I_0}^B$$

$$\dot{\hat{\mathbf{b}}} = -k_I\mathbf{y}_m, \quad \mathbf{y}_m = \left(\mathbf{a}_m^B \times \hat{\mathbf{a}}_m^B + \boldsymbol{\psi}_m^B \times \hat{\boldsymbol{\psi}}_m^B\right) \tag{15}$$

where, $k_p, k_I > 0$ are tuning gains, $\hat{\mathbf{b}}$ denotes an estimate of $\mathbf{b} = \mathbf{b}_1 + \mathbf{b}_2$, where $(\mathbf{b}_1, \mathbf{b}_2)$ are defined below Eq. (3).

Furthermore, $\hat{\mathbf{a}}_m^B = \hat{\mathcal{R}}_I^B \mathbf{a}_m^I$ and $\hat{\boldsymbol{\psi}}_m^B = \hat{\mathcal{R}}_I^B \boldsymbol{\psi}_m^I$. Then $\tilde{\mathcal{R}}_I^B \equiv \mathcal{R}_I^B - \hat{\mathcal{R}}_I^B$, $\tilde{\mathbf{b}} \equiv \mathbf{b} - \hat{\mathbf{b}}$, exponentially converge to $(I_3,\ 0_3)$.

4) INS/GPS Split Architecture (NCF+EKF): The novel INS/GPS split architecture proposed in this paper involves splitting the state vector in Section II-B such that (ψ, θ, ϕ), $\left(b_{1_p}, b_{1_q}, b_{1_r}\right)$ are estimated via the NCF (AHRS formulation) while (λ, μ, h), (v_n, v_e, v_d) and $\left(b_{a_x}, b_{a_y}, b_{a_z}\right)$ are estimated via an EKF. First the NCF solution is obtained and then the Euler angle estimates are fed into the EKF architecture to obtain the estimates of position and velocity. Implementing an EKF or a UKF for the 15 state INS/GPS model with the measurements given in Remark 2.8 can potentially lead to unobservability of some of the states of the system. For the INS/GPS model *without* bias this is not an issue. However, with the inclusion of bias as states in the EKF model and without increasing the dimension of the measurement matrix to compensate for the increase in the dimensionality of the state vector, loss of observability is not uncommon. Hence in order to avoid this, we consider the split architecture. We show through simulations that by the split architecture there is no loss of observability for the entire time of simulation. Furthermore, we specifically choose the NCF as the filter to estimate the Euler angles over the EKF or the UKF since the NCF is more robust to *unmodeled* gyroscopic bias [7] and requires lesser number of tuning parameters. The proposed INS/GPS fusion split architecture is shown in Figure 1.

It must be noted that accelerometer biases are not accounted for in the measurement model for the NCF in Figure 1. It was observed, for the scenario simulated in the paper, that this is not significant. However, in scenarios where accelerometer biases need to be accounted for, one could implement a single step time delay smoother, where the accelerometer bias estimated from the EKF is fed back to the NCF, which in turn feeds forward the attitude estimates to the EKF.

IV. Simulation Scenario

A 6 degree-of-freedom (DOF) model adapted from the open-source Flight Dynamics and Control toolbox (FDC) [9], [12] is used for the simulation study. The true AHRS state vector of the aircraft is set to $\psi(0) = 0°, \theta(0) = 20°, \phi(0) = 0°$, while the true INS/GPS state vector is set to $\lambda(0) = 0°, \mu(0) = 20°, h(0) = 100\ m$, $v_n(0) = 10\ m/s, v_e(0) = v_d(0) = 0\ m/s$ and $\psi(0) = 0°, \theta(0) = 20°, \phi(0) = 0°$. The accelerometer and rate gyroscope biases are initialized at 0. For each of the problems (AHRS, INS/GPS), 1000 Monte Carlo runs were generated and the root mean square error (RMSE) plots for the Euler angles in case of the AHRS and the position, velocity and Euler angles in case of the INS/GPS formulation are shown for $500\ s$ with $\Delta t = 0.025\ s$.

Sensor Noise Parameters: The rate gyroscope, accelerometer, magnetometer and GPS noise parameters, used to generate sensor data, are given as follows: $\sigma_p = \sigma_q = \sigma_r = 0.05°/s$, $\sigma_{1_p} = \sigma_{1_q} = \sigma_{1_r} = 0.05°/s$, $\sigma_{2_p} = \sigma_{2_q} = \sigma_{2_r} = 0.05°/s$, $\sigma_{a_x} = \sigma_{a_y} = \sigma_{a_z} = 0.1m/s^2$, $\sigma_\psi = 0.5°$, $\sigma_\lambda = \sigma_\mu = 10^{-7}\ deg$, $\sigma_h = 10\ m$ and $\sigma_{x_{gps}} = \sigma_{y_{gps}} = \sigma_{z_{gps}} = 0.1m/s$.

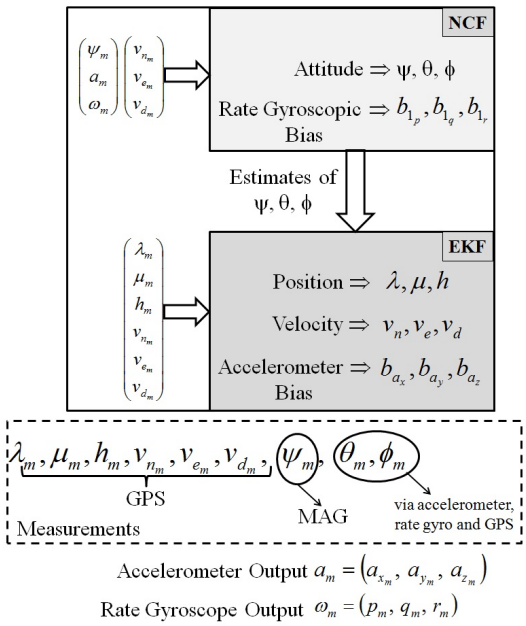

Fig. 1. Schematic of the INS/GPS Split Architecture: NCF+EKF.

The time constant for the colored noise process is chosen as $\tau = 100\,\text{s}$, $f_u = 5\,\text{Hz}$, while the inertial update rate is $40\,\text{Hz}$.

AHRS Simulation Results: For the 3 filters, $\hat{\mathbf{x}}(0) = 0_{6\times1} \Rightarrow$ for the NCF, $\hat{\mathcal{R}}_I^B(0) = I_3$. The EKF[9] and the UKF tuning parameters are $Q_{ekf} = \texttt{blkdiag}\left[\left(\frac{0.05\pi}{180}\right)^2 I_3\ \left(\frac{0.005\pi}{180}\right)^2 I_3\right], Q_{ukf} = \texttt{blkdiag}\left[\left(\frac{0.05\pi}{180}\right)^2 I_3\ \left(\frac{0.0005\pi}{180}\right)^2 I_3\right], P_{0_{ekf}} = P_{0_{ukf}} = \texttt{blkdiag}\left[\left(\frac{5\pi}{180}\right)^2 I_3\ \left(\frac{0.1\pi}{180}\right)^2 I_3\right]$, where `blkdiag` refers to a block diagonal matrix and $R_k = \left(\frac{0.5\pi}{180}\right)^2 I_3$. For the NCF, $k_P = 1, k_I = 0.1$ and for the UKF, $\alpha = 0.1,\ \beta = 2,\ \kappa = 0$. Figures 2 and 3 show the RMSE performance of the EKF, the UKF and the NCF in estimating the Euler angles and a sample plot of the rate gyroscopic bias respectively. It can be seen that the NCF outperforms either the EKF or the UKF. While the EKF and the UKF only estimate the $\mathbf{b}_1$ (Remark 2.2), the NCF estimates $\mathbf{b}_1 + \mathbf{b}_2$. Figure 4 shows the measurement histories for the EKF, UKF and NCF. For the EKF or the UKF, the measurements are ψ, θ, ϕ which are obtained as described in Eqs. (6) and (7). For the NCF, the measurements are ψ and an inertial estimate of the gravity vector. Ideally, this value should be $\begin{bmatrix} 0 & 0 & 9.81 \end{bmatrix}^T$ throughout, denoted by solid line in Figures 4(f) and (i). In Figure 4, notice that $g_1(t), g_2(t) \approx 0, \forall\ t \geq 0$ while $g_3(t)$ is distributed around $1g = 9.81\ m/s^2\ \forall\ t \geq 0$. The dashed curves in the Figure 4(d), (e), (g) and (h) represent the true values of θ, ϕ, while the corresponding solid curves are the measurements that the EKF uses.

INS/GPS Split Architecture Simulation Results: The INS/GPS split architecture is implemented by designing

[9]In [6], a performance comparison between the EKF and an error state Kalman filter is shown.

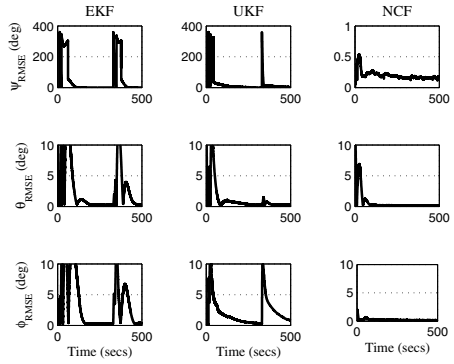

Fig. 2. RMSE of Euler Angles - AHRS Formulation.

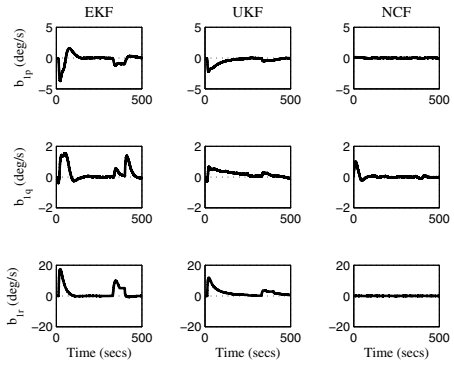

Fig. 3. A Sample Plot of Rate Gyro Bias Errors - AHRS Formulation.

an NCF for the Euler angles and an EKF for position and velocity. The initial state estimate for the NCF and EKF portions are set to 0. The EKF matrices are $Q_{ekf} = 0.01I_6, P_{0_{ekf}} = \texttt{blkdiag}\left[\left(\frac{10\pi}{180}\right)^2 I_2 \;\; 100^2 \;\; 25I_3 \;\; 0.25I_3\right]$ and $R_k = \left[\left(\frac{\pi}{180}\right)^2 I_2 \;\; 10^2 \;\; 0.1I_3 \;\; \left(\frac{0.5\pi}{180}\right)^2\right]$. For the NCF, $k_P = 1, k_I = 0.1$. Figure 5 shows the observability matrix rank for the entire simulation time history. It can be seen that in the case of a full EKF based INS/GPS formulation,

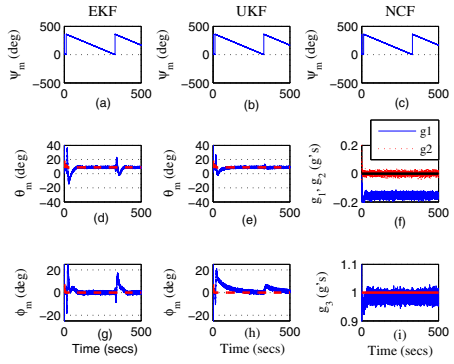

Fig. 4. AHRS Measurements: EKF, UKF and NCF.

the highest rank of the observability matrix is 13 while the dimension of the state vector is 15 $\Rightarrow$ loss of observability. However, by employing the split architecture observability is maintained for the NCF and the EKF portions individually. Furthermore, we observe from the RMSE performance of the inertial states in Figure 6 and a sample plot of the accelerometer and rate gyroscope biases in Figure 7 that the performance of the split architecture is more than acceptable.

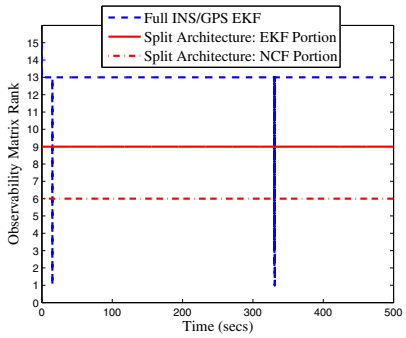

Fig. 5. Nonlinear Observability Matrix Rank Condition.

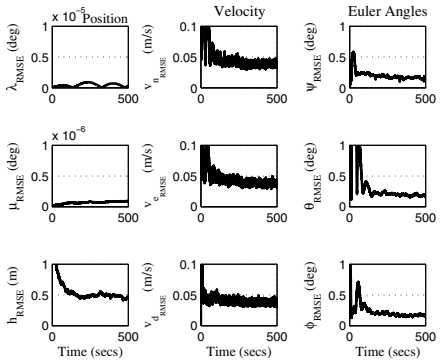

Fig. 6. RMSE of Position, Velocity and Euler Angles: NCF+EKF.

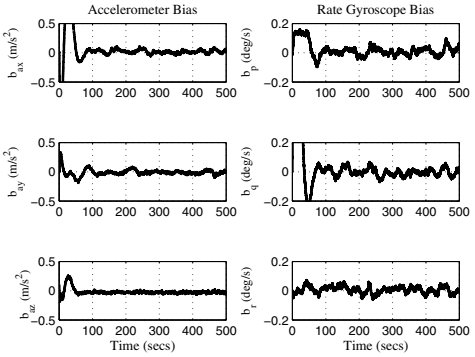

Fig. 7. Sample Plot of Accelerometer & Rate Gyroscope Bias Errors: NCF+EKF.

V. CONCLUSIONS

We have studied the performances of the extended Kalman filter (EKF), the unscented Kalman filter (UKF) and the nonlinear complementary filter (NCF) in estimating the Euler angles of an aircraft (AHRS) in the presence of unmodeled gyroscopic bias. Our study indicates that in the presence of unmodeled bias, the NCF shows superior performance to both the EKF and the UKF. Furthermore, we have also shown, via a nonlinear observability analysis, that the AHRS problem with accelerometer bias is not observable. *Lastly, based on our studies of the NCF, we have proposed a novel INS/GPS fusion architecture which exploits the robustness of the NCF in estimating the Euler angles in the presence of unmodeled rate gyroscopic bias, while employing an EKF to estimate the position and velocity in the presence of accelerometer bias.*

Appendix A: Nonlinear Observability

Consider the following nonlinear dynamical system

$$\begin{aligned}\dot{\bar{\mathbf{x}}}(t) &= \bar{\mathbf{f}}(\bar{\mathbf{x}}(t)) = \begin{bmatrix} \bar{f}_1(\bar{\mathbf{x}}(t)) & \dots & \bar{f}_n(\bar{\mathbf{x}}(t)) \end{bmatrix}^T \\ \bar{\mathbf{z}}(t) &= \bar{\mathbf{h}}(\bar{\mathbf{x}}(t)) = \begin{bmatrix} \bar{h}_1(\bar{\mathbf{x}}(t)) & \dots & \bar{h}_p(\bar{\mathbf{x}}(t)) \end{bmatrix}^T \end{aligned} \quad (16)$$

where, $\bar{\mathbf{x}} \in \mathcal{R}^n$ is the $n-$dimensional state of the system, $\bar{\mathbf{z}} \in \mathcal{R}^p$ is the $p-$dimensional system measurement, $\bar{\mathbf{f}} : \mathcal{R}^n \rightarrow \mathcal{R}^n$ is the nonlinear mapping of the system states called as the system dynamics such that $\bar{f}_i \in \mathcal{R}^n \rightarrow \mathcal{R},\ i = 1, 2, \dots, n$ and $\bar{\mathbf{h}} : \mathcal{R}^n \rightarrow \mathcal{R}^p$ is the nonlinear mapping of the system states to the measurement such that $\bar{h}_j \in \mathcal{R}^n \rightarrow \mathcal{R},\ j = 1, 2, \dots, p$. The vector of measurements and its time derivatives up to and including $n-1$ is formed as

$$\boldsymbol{\mathcal{Z}} = \begin{bmatrix} \bar{\mathbf{z}} \\ \dot{\bar{\mathbf{z}}} \\ \vdots \\ \bar{\mathbf{z}}^{n-1} \end{bmatrix} = \begin{bmatrix} L^0_{\bar{\mathbf{f}}}(\bar{\mathbf{h}}) \\ L^1_{\bar{\mathbf{f}}}(\bar{\mathbf{h}}) \\ \vdots \\ L^{n-1}_{\bar{\mathbf{f}}}(\bar{\mathbf{h}}) \end{bmatrix} = \bar{\mathbf{g}}_{\bar{\mathbf{z}}}(\bar{\mathbf{x}}) \quad (17)$$

where, $\bar{\mathbf{z}}^{n-1}$ denotes the $(n-1)^{st}$ time derivative of $\bar{\mathbf{z}}$, $L^0_{\bar{\mathbf{f}}}(\bar{\mathbf{h}}), \cdots, L^{n-1}_{\bar{\mathbf{f}}}(\bar{\mathbf{h}})$ denote the Lie derivatives [20] of the measurement and $\bar{\mathbf{g}}_{\bar{\mathbf{z}}}(\cdot) : (\bar{\mathbf{x}} \in \mathcal{R}^n) \rightarrow \mathcal{R}^{np\times 1}$. The Lie derivatives are given by

$$L^1_{\bar{\mathbf{f}}} = \begin{bmatrix} \underbrace{\Sigma_{i=1}^n \frac{\partial \bar{h}_1}{\partial \bar{x}_i}\bar{f}_i}_{L^1_{1_{\bar{\mathbf{f}}}}} \\ \vdots \\ \underbrace{\Sigma_{i=1}^n \frac{\partial \bar{h}_p}{\partial \bar{x}_i}\bar{f}_i}_{L^1_{p_{\bar{\mathbf{f}}}}} \end{bmatrix}, \dots, L^{n-1}_{\bar{\mathbf{f}}} = \begin{bmatrix} \underbrace{\Sigma_{i=1}^n \frac{\partial L^{n-2}_{1_{\bar{\mathbf{f}}}}}{\partial \bar{x}_i}\bar{f}_i}_{L^{n-1}_{1_{\bar{\mathbf{f}}}}} \\ \vdots \\ \underbrace{\Sigma_{i=1}^n \frac{\partial L^{n-2}_{p_{\mathbf{f}}}}{\partial \bar{x}_i}\bar{f}_i}_{L^{n-1}_{p_{\bar{\mathbf{f}}}}} \end{bmatrix} \quad (18)$$

Furthermore, $L^0_{\bar{\mathbf{f}}} = \bar{\mathbf{h}}(\bar{\mathbf{x}}(t))$. Taking the Taylor series of Eq. (17) about $\bar{\mathbf{x}}^*$ and neglecting the higher order terms, we obtain

$$\begin{aligned}\boldsymbol{\mathcal{Z}} &= \bar{\mathbf{g}}_{\bar{\mathbf{z}}}(\bar{\mathbf{x}}) = \bar{\mathbf{g}}_{\bar{\mathbf{z}}}(\bar{\mathbf{x}}^*) + \underbrace{\left.\frac{\partial \bar{\mathbf{g}}_{\bar{\mathbf{z}}}(\bar{\mathbf{x}})}{\partial \bar{\mathbf{x}}}\right|_{\bar{\mathbf{x}}=\bar{\mathbf{x}}^*}}_{\mathcal{O}(\bar{\mathbf{x}}^*)\in\mathcal{R}^{np\times n}}(\bar{\mathbf{x}} - \bar{\mathbf{x}}^*) \\ \Rightarrow \bar{\mathbf{x}} &= \bar{\mathbf{x}}^* + \left(\mathcal{O}^T\mathcal{O}\right)^{-1}\ \mathcal{O}^T\left(\boldsymbol{\mathcal{Z}} - \bar{\mathbf{g}}_{\bar{\mathbf{z}}}(\bar{\mathbf{x}}^*)\right) \end{aligned} \quad (19)$$

where, $\mathcal{O}$ is called as the observability matrix. From Eq. (19) it can be easily seen that $\mathcal{O}^T\mathcal{O} \in \mathcal{R}^{n\times n}$ is invertible if $rank\left(\mathcal{O}^T\mathcal{O}\right) = n$. This is called as the *nonlinear observability rank condition*. Since the higher order Taylor series terms were ignored in order to arrive at the expression in Eq. (19), observability for nonlinear systems is confined to a local domain around the point or vector (in the case of non-scalar systems) $\bar{\mathbf{x}}^*$. In the case of linear systems, with $\bar{\mathbf{f}}(\bar{\mathbf{x}}) = A\bar{\mathbf{x}}$, $\bar{\mathbf{h}}(\bar{\mathbf{x}}) = C\bar{\mathbf{x}}$, the notion of observability is global.

Observability Analysis: AHRS, X-axis Accelerometer Bias, No Gyro Bias, 3 Measurements: We examine the nonlinear observability condition of the AHRS model with only the X-axis accelerometer bias and without modeling gyroscopic bias. The measurements used are ψ, θ and ϕ. The state vector is $\bar{\mathbf{x}} = \begin{bmatrix} \psi & \theta & \phi & b_{a_x} \end{bmatrix}^T \Rightarrow n = 4$, where b_{a_x} is the bias in a_{x_m}. We assume that $b_{a_y} = b_{a_z} = 0$, $b_{1_p} = b_{1_q} = b_{1_r} = 0$, $b_{2_p} = b_{2_q} = b_{2_r} = 0$ and $b_{w_p} = b_{w_q} = b_{w_r} = 0$. Furthermore, assume that b_{a_x} is modeled as a first order Gauss-Markov processes such that $\dot{b}_{a_x} = -\frac{b_{a_x}}{\tau_a} + \frac{w_{a_x}}{\tau_a}$, where, w_{a_x} is a 0 mean, band-limited AWGN process of specified covariance and τ_a is the process time constant. The AHRS model collapses to

$$\begin{bmatrix} \dot{\psi} \\ \dot{\theta} \\ \dot{\phi} \\ \dot{b}_{a_x} \end{bmatrix} = \begin{bmatrix} \underbrace{q\frac{s_\phi}{c_\theta} + r\frac{c_\phi}{c_\theta}}_{\bar{f}_1} \\ \underbrace{qc_\phi - rs_\phi}_{\bar{f}_2} \\ \underbrace{p + qs_\phi t_\theta + rc_\phi t_\theta}_{\bar{f}_3} \\ -\frac{b_{a_x}}{\tau_a} \end{bmatrix} + \begin{bmatrix} 0 \\ 0 \\ 0 \\ \frac{1}{\tau_a} \end{bmatrix} w_{a_x} \quad (20)$$

Furthermore, we make use of the following expressions:

$$\begin{aligned}\frac{\partial \bar{f}_1}{\partial \psi} &= 0, \frac{\partial \bar{f}_1}{\partial \theta} = \bar{f}_1 t_\theta, \frac{\partial \bar{f}_1}{\partial \phi} = \frac{\bar{f}_2}{c_\theta}, \quad \frac{\partial \bar{f}_2}{\partial \psi} = 0, \frac{\partial \bar{f}_2}{\partial \theta} = 0 \\ \frac{\partial \bar{f}_2}{\partial \phi} &= -\bar{f}_1 c_\theta, \quad \frac{\partial \bar{f}_3}{\partial \psi} = 0, \frac{\partial \bar{f}_3}{\partial \theta} = \frac{\bar{f}_1}{c_\theta}, \frac{\partial \bar{f}_3}{\partial \phi} = \bar{f}_2 t_\theta \end{aligned} \quad (21)$$

Thus with Eq. (21), the Lie derivatives are computed as $L^0_{\bar{\mathbf{f}}} = \begin{bmatrix} \psi & \theta & \phi \end{bmatrix}^T$, $L^1_{\bar{\mathbf{f}}} = \begin{bmatrix} \bar{f}_1 & \bar{f}_2 & \bar{f}_3 \end{bmatrix}^T$, $L^2_{\bar{\mathbf{f}}} = \begin{bmatrix} \bar{f}_1\bar{f}_2 t_\theta + \frac{\bar{f}_2\bar{f}_3}{c_\theta} & -\bar{f}_1\bar{f}_3 c_\theta & \frac{\bar{f}_1\bar{f}_2}{c_\theta} + \bar{f}_2\bar{f}_3 t_\theta \end{bmatrix}^T$ and $L^3_{\bar{\mathbf{f}}} = \begin{bmatrix} L^3_{1_{\bar{\mathbf{f}}}} & L^3_{2_{\bar{\mathbf{f}}}} & L^3_{3_{\bar{\mathbf{f}}}} \end{bmatrix}^T$, where, $L^3_{1_{\bar{\mathbf{f}}}} = \frac{\bar{f}_1\bar{f}_2^2}{c_\theta^2}\left(2 + s_\theta^2\right) + 3\bar{f}_2^2\bar{f}_3\frac{t_\theta}{c_\theta} - \bar{f}_1\left(\bar{f}_1 s_\theta + \bar{f}_3^2\right)$, $L^3_{2_{\bar{\mathbf{f}}}} = -\bar{f}_2\left(\bar{f}_1^2 + \bar{f}_3^2 + \bar{f}_1\bar{f}_3 s_\theta\right)$ and $L^3_{3_{\bar{\mathbf{f}}}} = \frac{\bar{f}_2^2}{c_\theta^2}\left(\bar{f}_1 + 2\bar{f}_3 + 2\bar{f}_1 s_\theta\right) + \bar{f}_3\left(\bar{f}_2^2 t_\theta^2 - \bar{f}_1^2 - \bar{f}_1\bar{f}_3 s_\theta\right)$, which then yields $\bar{\mathbf{g}}_{\bar{\mathbf{z}}}(\bar{\mathbf{x}})$. At this point to obtain $\mathcal{O}$ and then $\mathcal{O}^T\mathcal{O}$, we use the symbolic toolbox in MATLAB, which results in $\mathcal{O} \in \mathcal{R}^{12\times 4}$. Furthermore, a simple $\mathcal{O}^T\mathcal{O} \in \mathcal{R}^{4\times 4}$ operation in MATLAB shows that all the entries of the 4^{th} row of $\mathcal{O}^T\mathcal{O}$ are 0. Thus, $rank\left(\mathcal{O}^T\mathcal{O}\right) < 4 \Rightarrow$ the system in Eq. (20) with $\bar{\mathbf{z}} = \begin{bmatrix} \psi & \theta & \phi \end{bmatrix}^T$ is *unobservable*. **Thus, for the AHRS formulation, accelerometer bias is not considered.**

Appendix B: $\mathbf{x}$, $\mathbf{f}$ *and non-zero entries of* F *&* Γ *matrices*

1) AHRS: $\mathbf{x} = \begin{bmatrix} \boldsymbol{\xi}^T & \mathbf{b}_1^T \end{bmatrix}^T$ and $\mathbf{f} = \begin{bmatrix} \boldsymbol{\omega}_m^T \Lambda^T & \mathbf{0}_{1\times 3} \end{bmatrix}^T$. The Jacobian matrix entries are: $F_{[1,2]} = \frac{\kappa_{21} s_\theta}{c_\theta^2}, F_{[1,3]} = \frac{\kappa_{22}}{c_\theta}, F_{[1,5]} = \frac{s_\phi}{c_\theta}, F_{[1,6]} = \frac{c_\phi}{c_\theta}, F_{[2,3]} = -\kappa_{21}, F_{[2,5]} = c_\phi, F_{[2,6]} = -s_\phi, F_{[3,2]} = \frac{\kappa_{21}}{c_\theta^2}, F_{[3,3]} = \kappa_{22} t_\theta, F_{[3,4]} = 1, F_{[3,5]} = s_\phi t_\theta, F_{[3,6]} = c_\phi t_\theta$, where, $\kappa_{21} = \left(q + b_{1_q}\right) s_\phi + \left(r + b_{1_r}\right) c_\phi$, $\kappa_{22} = \left(q + b_{1_q}\right) c_\phi - \left(r + b_{1_r}\right) s_\phi$. The Γ matrix entries are: $\Gamma_{[1,2]} = \frac{s_\phi}{c_\theta}, \Gamma_{[1,3]} = \frac{c_\phi}{c_\theta}, \Gamma_{[2,2]} = c_\phi, \Gamma_{[2,3]} = -s_\phi, \Gamma_{[3,2]} = s_\phi t_\theta, \Gamma_{[3,3]} = c_\phi t_\theta, \Gamma_{[3,1]} = \Gamma_{[4,4]} = \Gamma_{[5,5]} = \Gamma_{[6,6]} = 1$.

2) INS/GPS: $\mathbf{x} = \begin{bmatrix} \mathbf{p}_I^T & \mathbf{v}_I^T & \boldsymbol{\xi}^T & \mathbf{b}_1^T & \mathbf{b}_a^T \end{bmatrix}^T$, where $\mathbf{b}_a = \begin{bmatrix} b_{a_x} & b_{a_y} & b_{a_z} \end{bmatrix}^T$ and $\mathbf{f} = \begin{bmatrix} \mathbf{f}_1^T & \mathbf{f}_2^T & \boldsymbol{\omega}_m^T \Lambda^T & \mathbf{0}_{1\times 6} \end{bmatrix}^T$, $\mathbf{0}_{1\times 6}$ is a 1×6 zero vector. The Jacobian matrix entries are: $F_{[1,1]} = -\frac{v_n R_{M_\lambda}}{\alpha_M^2}, F_{[1,3]} = -\frac{v_n}{\alpha_M^2}, F_{[1,4]} = \frac{1}{\alpha_M}, F_{[2,1]} = \frac{v_e\left(\alpha_N s_\lambda - R_{N_\lambda} c_\lambda\right)}{\alpha_N^2 c_\lambda^2}, F_{[2,3]} = -\frac{v_e}{\alpha_N^2 c_\lambda}, F_{[2,5]} = \frac{1}{\alpha_N c_\lambda}, F_{[3,6]} = -1, F_{[4,1]} = -\frac{v_n v_d R_{M_\lambda}}{\alpha_M^2} - \frac{v_e^2}{\alpha_N^2}\left(\frac{\alpha_N}{c_\lambda^2} - t_\lambda R_{N_\lambda}\right), F_{[4,3]} = -\frac{v_n v_d}{\alpha_M^2} + \frac{v_e^2 t_\lambda}{\alpha_N^2}, F_{[4,4]} = \frac{v_d}{\alpha_M}, F_{[4,5]} = -\frac{2 v_e t_\lambda}{\alpha_N}, F_{[4,6]} = \frac{v_n}{\alpha_M}, F_{[4,7]} = \mathcal{R}^I_{B_{[1,1]}}, F_{[4,8]} = \mathcal{R}^I_{B_{[1,2]}}, F_{[4,9]} = \mathcal{R}^I_{B_{[1,3]}}, F_{[5,1]} = -\frac{v_e v_d R_{N_\lambda}}{\alpha_N^2} + \frac{v_e v_n}{\alpha_N^2}\left(\frac{\alpha_N}{c_\lambda^2} - t_\lambda R_{N_\lambda}\right), F_{[5,3]} = -\frac{v_e}{\alpha_N^2}\left(v_d + v_n t_\lambda\right), F_{[5,4]} = \frac{v_e t_\lambda}{\alpha_N}, F_{[5,5]} = \frac{v_d + v_n t_\lambda}{\alpha_N}, F_{[5,6]} = \frac{v_e}{\alpha_N}, F_{[5,7]} = \mathcal{R}^I_{B_{[2,1]}}, F_{[5,8]} = \mathcal{R}^I_{B_{[2,2]}}, F_{[5,9]} = \mathcal{R}^I_{B_{[2,3]}}, F_{[6,1]} = \frac{v_d^2 R_{M_\lambda}}{\alpha_M^2} + \frac{v_e^2 R_{N_\lambda}}{\alpha_N^2}, F_{[6,3]} = \frac{v_d^2}{\alpha_M^2} + \frac{v_e^2}{\alpha_N^2}, F_{[6,5]} = -\frac{2 v_e}{\alpha_N}, F_{[6,6]} = -\frac{2 v_d}{\alpha_M}, F_{[6,7]} = \mathcal{R}^I_{B_{[3,1]}}, F_{[6,8]} = \mathcal{R}^I_{B_{[3,2]}}, F_{[6,9]} = \mathcal{R}^I_{B_{[3,3]}}$, where $R_{M_\lambda} = 3\alpha_\lambda R_M, R_{N_\lambda} = \alpha_\lambda R_N, \alpha_\lambda = \frac{e^2 s_\lambda c_\lambda}{\gamma^2}, \alpha_M = R_M + h, \alpha_N = R_N + h, \gamma = \sqrt{1 - e^2 s_\lambda^2}$. The Γ matrix is $\Gamma = \texttt{blkdiag}\left[\mathcal{R}_B^I \; I_3\right]$.

REFERENCES

[1] Y. Bar-Shalom, X. Rong Li and T. Kirubarajan, *Estimation with Applications to Tracking and Navigation*, Wiley-Interscience, 2003.

[2] J.L. Crassidis, F.L. Markley and Y. Cheng, "A Survey of Nonlinear Attitude Estimation Methods", *AIAA Journal of Guidance, Control and Dynamics*, Vol. 30, No. 1, pp. 12-28, 2007.

[3] F. Daum, "Nonlinear filters: beyond the Kalman filter", IEEE Aerospace and Electronic Systems Magazine, Vol. 20, No. 8, pp. 57 - 69, Aug. 2005.

[4] P. Eykhoff, *System Identification*, Wiley, 1974.

[5] A.H. Jazwinski, *Stochastic Processes and Filtering Theory*, New York, Academic, 1970.

[6] V.K. Madyastha, V.C. Ravindra, S. Mallikarjunan and A. Goyal, "Extended Kalman Filter vs. Error State Kalman Filter for Aircraft Attitude Estimation", in *AIAA GNC*, Portland, Oregon, 2011.

[7] R. Mahony, T. Hamel and J-M Pflimlin, "Nonlinear Complementary Filters on the Special Orthogonal Group", *IEEE Transactions on Automatic Control*, Vol. 53, No. 5, pp. 1203-1218, 2008.

[8] H. Nijmeijer and T. Fossen, *New directions in nonlinear observer design*, (Eds.) Lecture Notes in Control and Information Sciences 244, Springer Verlag, London, 1999.

[9] M. Rauw, "FDC1.2 - A SIMULINK toolbox for flight dynamics and control analysis", *Technical Report*, 2001.

[10] R. van der Merwe, *Sigma-Point Kalman Filters for Probabilistic Inference in Dynamic State Space Models*, Doctoral Dissertation, Oregon Health & Science University, 2004.

[11] ANTARIS Protocol Specification, *Ublox*, `http://www.u-blox.com/en/download/documents-a-resources/antaris-4-gps-modules-resources`.

[12] The Flight Dynamics & Control Toolbox, `http://92.254.81.198`.

[13] M. Athans, R.P. Wishner, A. Bertolini, "Suboptimal State Estimation for Continuous Time Nonlinear Systems from Discrete Noisy Measurements", *IEEE Transactions on Automatic Control*, Vol. AC - 13, 1968.

[14] B. Barshan and H. F. Durrant-Whyte, "Inertial navigation systems for mobile robots", *IEEE Transactions on Robotics and Automation*, Vol. 11, No. 3, pp. 328 - 342, June 1995.

[15] S. Bonnabel and P. Rouchon, "A non-linear symmetry-preserving observer for velocity-aided inertial navigation", *American Control Conference*, pp. 2910-2914, June 2006.

[16] E. Brookner, "The Multifaceted Peter Swerling", *IEEE AESS Systems Magazine*, June, 2001.

[17] R. Brown and P. Hwang, *Introduction to Random Signals and Applied Kalman Filtering*, John Wiley and Sons, Inc., 1992.

[18] O. Egland and J. Godhaven, "Passivity based adaptive attitude control of a rigid spacecraft", *IEEE Transactions on Automatic Control*, Vol. 39, pp. 842-846, 1994.

[19] B. Etkin and L.D. Reid, *Dynamics of Flight Stability and Control*, 3^{rd} Edition, John Wiley and Sons, Inc., 1996.

[20] A. Isidori, *Nonlinear Control Systems*, Springer, Berlin, 1995.

[21] S.J. Julier, J.K. Uhlmann and H.F. Durrant-Whyte, "A New Approach for Filtering Nonlinear Systems", *Proceedings of American Controls Conference*, 1628-1632, 1995.

[22] S.J. Julier and J.K. Uhlmann, "A New Extension of the Kalman Filter to Nonlinear Systems", *Proceedings of AeroSense: The* 11^{th} *International Symposium on Aerospace/Defense Sensing, Simulation and Controls, Multi Sensor Fusion, Tracking and Resource Management II, SPIE*, 1997.

[23] R.E. Kalman, "A New Approach to Linear Filtering and Prediction Problems", *Transactions of the ASME - Journal of Basic Engineering*, 82 (Series D): 35-45, 1960.

[24] S.E. Lyshevski, *MEMS and NEMS: Systems, Devices and Structures*, CRC Press, 2002.

[25] S.I. Roumeliotis, G.S. Sukhatme, and G.A. Bekey, "Circumventing Dynamic Modeling: Evaluation of the Error-State Kalman Filter Applied to Mobile Robot Localization", in *IEEE Intl. Conf. on Robot Localization*, pp. 1656 - 1663, Michigan, May 1999.

[26] S. Salcudean, "A globally convergent angular velocity observer for rigid body motion", *IEEE Transactions on Automatic Control*, Vol. 36, No. 12, pp. 1493-1497, 1991.

[27] O.S. Salychev, Applied Inertial Navigation Problems and Solutions, BMSTU Press, Moscow, 2004.

[28] G.T. Schmidt and R.E. Phillips, "INS/GPS Integration Architecture Performance Comparisons", *Draper Lab Report*, P-4105, MA, 2003.

[29] P. Swerling, "First Order Error Propagation in a Stagewise Smoothing Procedure for Satellite Observations", *Journal of the Astronomical Sciences*, Vol. 6, No. 3, Autumn 1959.

[30] J. Thienel and R. M. Sanner, "A coupled nonlinear spacecraft attitude controller and observer with an unknown constant gyro bias and gyro noise", *IEEE Transactions on Automatic Control*, Vol. 48, No. 11, pp. 2011-2015, 2003.

[31] D.H. Titterton and J.L. Weston, *Strapdown Inertial Navigation Technology*, IEE, 1997.

[32] O. Woodman, "An Introduction to Inertial Navigation", Technical Report 696, University of Cambridge, 2007.